analytical chemistry

Article

pubs.acs.org/ac

Fused Deposition Modeling 3D Printing for (Bio)analytical Device Fabrication: Procedures, Materials, and Applications

Gert IJ. Salentijn,[†,‡] Pieter E. Oomen,[†] Maciej Grajewski,[†] and Elisabeth Verpoorte*[,†]

[†]Pharmaceutical Analysis, Groningen Research Institute of Pharmacy, University of Groningen, 9700 AD Groningen, The Netherlands

[‡]TI-COAST, Science Park 904, 1098 XH Amsterdam, The Netherlands

Supporting Information

ABSTRACT: In this work, the use of fused deposition modeling (FDM) in a (bio)analytical/lab-on-a-chip research laboratory is described. First, the specifications of this 3D printing method that are important for the fabrication of (micro)devices were characterized for a benchtop FDM 3D printer. These include resolution, surface roughness, leakage, transparency, material deformation, and the possibilities for integration of other materials. Next, the autofluorescence, solvent compatibility, and biocompatibility of 12 representative FDM materials were tested and evaluated. Finally, we demonstrate the feasibility of FDM in a number of important applications. In particular, we consider the fabrication of fluidic channels, masters for polymer replication, and tools for the production of paper microfluidic devices. This work thus provides a guideline for (i) the use of FDM technology by addressing its possibilities and current limitations, (ii) material selection for FDM, based on solvent compatibility and biocompatibility, and (iii) application of FDM technology to (bio)analytical research by demonstrating a broad range of illustrative examples.

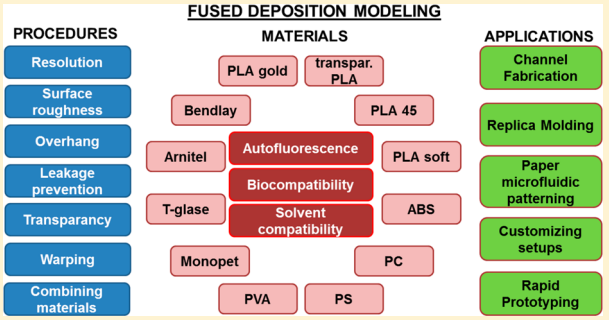

It is safe to say that scientists working in research laboratories are generally not self-sufficient when it comes to conducting experiments, regardless of the field of interest. For example, we all are dependent on external suppliers for consumables and labware, which means that these materials must be ordered periodically and in a timely fashion, often in bulk, and stored somewhere before use. If experiments involve lab-on-a-chip technology and instrumental techniques, we must often turn to a workshop when it comes to things such as customizing a microscope stage (for positioning a lab-chip, for example) or having clamping devices or alignment tools made. If the workshop is busy (as workshops often are), our experiment is delayed. Resorting to temporary solutions such as duct tape to align and fix components to do that experiment anyway generally just leads to additional delay. The iterative development of a (bio)analytical device using "rapid" prototyping approaches can be slowed significantly too if we are dependent on external partners or companies to perform certain processing steps. All these are recurring issues, or annoyances at the very least, to which we have often had to resign ourselves in the prototypical microfluidics laboratory. The bigger problem is, of course, that these inconveniences cause us to be inefficient against our will, meaning they cost time and money. Can we envision a world where we can shed our experimental dependence on these kinds of external factors? Perhaps we can—at least if we can master the new additive manufacturing techniques that constitute 3D printing.

3D printing is not a new technology, as it has been used in some industrial settings for over 30 years. However, 3D printing systems have tended to be very specialized and expensive until recently, making them relatively inaccessible for most potential end users. In addition, early equipment was often not very user-friendly, with long and relatively unreliable printing processes being typical. The history of 3D printing, as well as a comparative description of a number of different 3D printing approaches, has been nicely summarized in recent reviews.[1−6]

In the past few years, we have seen a rapid increase in publications on the use of 3D printing in (bio)analytical and microfluidics research.[2] It has been used for the fabrication of channels,[7−11] sample cartridges,[12] and masters for replication of channels in poly(dimethylsiloxane) (PDMS),[13−16] hydrophobic patterning in paper microfluidics,[17] and fabrication of labware and customized setups.[18−25] Furthermore, 3D-printed materials have been studied to some extent with respect to their physical properties[9,26] and biocompatibility in cell- or tissue-based assays.[18,21,25,27] As optical transparency is often a problem with 3D-printed lab-chip devices, incorporation of glass slides into these devices has also been reported.[25,27] These advances have been achieved with different 3D printing approaches, namely,

Received: March 6, 2017
Accepted: June 6, 2017
Published: June 19, 2017

DOI: 10.1021/acs.analchem.7b00828
Anal. Chem. 2017, 89, 7053−7061

stereolithography (SL), fused deposition modeling (FDM), inkjet 3D printing, digital light processing (DLP), and selective laser sintering (SLS). This means that the experience that researchers have with 3D printing for device fabrication is somewhat fragmented. It would therefore be useful to assess and characterize all these approaches individually, to allow for a better comparison of approaches and selection of the most suitable approach for a given application.

As a first step in this direction, we focus in this paper on 3D printing by FDM. We describe the technology and address its current possibilities and limitations with respect to (bio)analytical devices and, more generally, experimental research. Furthermore, this work contains an extensive table in which several important properties (including biocompatibility and solvent compatibility) of 12 representative FDM materials are listed, to aid in material selection for specific medical, biological, or chemical applications. Finally, we demonstrate the applicability of FDM to the fabrication of (bio)analytical (micro)devices and customization of experimental setups. All the examples in this paper were designed, fabricated, and implemented in our laboratory at the University of Groningen and are presented here to show the impact that 3D printing has had on our own "microenvironment".

FUSED DEPOSITION MODELING

FDM is based on the melting and extrusion of a polymer filament. The filament is fed into and melted in a heated metal cylinder ending in a nozzle. As fresh filament is supplied continuously into this component, the molten polymer is pushed out of the nozzle, forming a thread roughly the size of the nozzle diameter. To shape this thread into a plastic part, the nozzle is placed above a metal plate (*print bed*) at a distance that depends on the desired resolution. Upon exiting the nozzle, the filament is deposited on this print bed, which can be heated to promote attachment. When the print bed and nozzle are both controllably moved in perpendicular directions, we can draw a two-dimensional figure on the print bed having the thickness of one polymer thread. This thickness (generally between 0.1 and 0.3 mm) is controlled by (i) the distance between the nozzle and the print bed and (ii) the ratio between the flow rate of the filament through the nozzle and the printing speed. When the first layer is finished, the print bed is lowered by a fixed distance (i.e., the thickness of a single layer), and a second layer can be printed on top of the original one. By repeating these steps, an object is created in an additive manner.

To print a 3D-drawn model, it first needs to be translated to a file which guides printer operation. This process is described in detail by Gross and co-workers.[1] In short, the 3D drawing (often a vector file) is saved in the *.STL format, which is a triangular surface mesh. This file is then sliced into a path for the extruder to follow (generating a G-code); the solid model is thus converted into a digital equivalent of filament threads.

MATERIALS AND METHODS

Characterization of a Benchtop FDM 3D Printer. For the fabrication of the devices in this work, a Felix v.3.0 (FELIX printers, de Meern, The Netherlands, nozzle diameter 0.35 mm) was used. This FDM 3D printer was chosen because of its open and accessible architecture. SolidWorks (Waltham, MA) was used to design the 3D models for printing, which were then sliced using sFact/Skeinforge freeware. Repertier host freeware was used to control the 3D printer. We characterized this printer by considering (i) the resolution, surface roughness, and overhang, (ii) leakage prevention, (iii) the transparency, (iv) combination of materials in one printed object, and (v) object warping during printing (Supporting Information, protocols S1–S3).

Polymers for FDM 3D Printing. A number of physical and biological specifications of 12 FDM filament materials were assessed in this study (Supporting Information, protocols S4–S6). The materials with their respective printing parameters are listed in Table S2, Supporting Information. These 12 materials are representative of commercially available materials for FDM. They comprise different polymers and have varying degrees of elasticity. The materials were tested for (i) autofluorescence at three wavelengths (protocol S4), (ii) compatibility with different solvents (water, methanol, acetonitrile, 2-propanol, acetone) (protocol S5), and (iii) biocompatibility with a primary cell model (human umbilical vein endothelial cells (HUVECs)) and a rat tissue model (precision cut liver slices (PCLSs)) (protocol S6).

Biocompatibility in the context of this study refers to the material property that results in the viability of cells and tissue being unaffected when exposed to the material under in vitro culture conditions. A material that is not biocompatible will adversely affect cell or tissue viability in its proximity to some extent, resulting in altered cell behavior or even death. HUVEC cultures and PCLSs were exposed to the different 3D-printed materials for 18 and 24 h, respectively. One day of incubation is sufficient to assess whether the printed materials are toxic for the tested in vitro models.[28,29] Viability was assessed in HUVECs by microscopy and a test of metabolic activity (MTT test); viability in PCLSs was assessed by quantifying the adenosine triphosphate (ATP) content and lactate dehydrogenase (LDH) leakage into the medium. A material was considered biocompatible if the test results were not found to be statistically different from the results of the control experiment.

Applications of FDM 3D Printing. In the final part of this work, we tested the applicability of FDM to a number of common lab-on-a-chip/(bio)analytical applications. The applications that are considered in this work are (i) channel fabrication, (ii) channel replication in poly(dimethylsiloxane) (PDMS), (iii) paper microfluidic channel fabrication, and (iv) setup customization (Supporting Information, protocols S7 and S8).

RESULTS AND DISCUSSION

Characterization of a Benchtop FDM 3D Printer. *Resolution, Surface Roughness, and Overhang.* Resolution is an important issue with respect to the current generation of benchtop 3D printers if small (<100 μm) channels are desired. Most published examples of 3D-printed microchannels report channel sizes of a few hundred micrometers (e.g., 200–250 μm for DLP[9,10,30]). Figure 1 shows a 3D-printed object with channels of varying size and shape. Open channels with dimensions below 200 μm (400 μm by design) were obtained, which was ascertained by shining light through them. The difference between the actual and designed channel widths is a result of the tolerances of the printer. Positive structures (solid, protruding) are generally printed slightly larger, whereas negative structures (recessed, open/embedded) are slightly smaller. The surface and shape of these small channels are not so smooth, due to the fact that these dimensions are in the

DOI: 10.1021/acs.analchem.7b00828
Anal. Chem. 2017, 89, 7053–7061

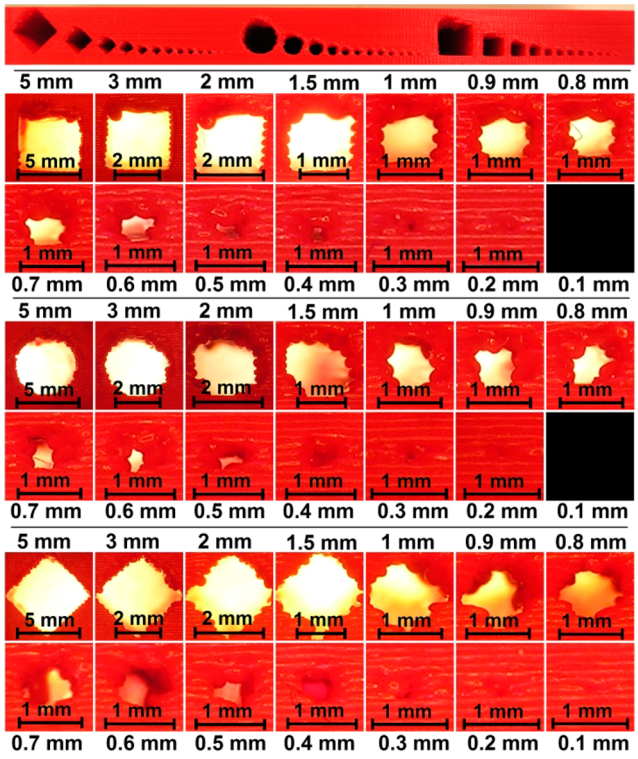

Figure 1. Resolution of FDM 3D-printed channels (rectangular, circular, and diamond-shaped). The top panel shows the front view of the entire test structure, presented in Figure S1, Supporting Information. The panels below depict enlarged views of the individual channels, all scaled individually to the size of the frame.

same range as the dimensions of a single thread of extruded material. Larger channels assume a more well-defined shape.

In other work on FDM, a channel with a diameter of 0.8 mm was successfully used in 3D-printed reactionware.[7] However, the effect of limited resolution due to the filament dimension is clearly visible in Figure 1 at this smaller scale. In larger channels, the microstructure of the fused threads of filament is identical to that of smaller channels, which means that these channels possess the same absolute surface roughness. However, the overall effect of individual filaments on the definition of the channel shape is much less pronounced, as can also be seen in Figure 1. This is inherent to the FDM process and should be taken into account when FDM is selected as a fabrication method. While it is clear that FDM is not suitable for direct fabrication of smooth microfluidic channels, it can be suitable for structures that are less dependent on the exact channel shape or can be operated on the millimeter scale (millifluidics).

Figure 1 also shows the quality of overhanging structures. Due to the nature of FDM, bridging structures are difficult to produce, as there are no layers supporting them. One solution to this problem is to print support structures (implemented into the G-code during slicing), which can be removed afterward. However, such structures are impossible to remove inside small channels. A second option is to use dual-head printing, in which the channel can be filled with a water-soluble material (e.g., poly(vinyl alcohol), PVA). The easiest solution (if applicable) is to use designs which circumvent this issue altogether. The overhang tends to start collapsing when its size exceeds a certain threshold. Below this threshold (more or less 1 mm; see Figure 1), collapse is not a problem. If a circular or diamond-shaped channel shape is chosen instead of a rectangular one, the overhang is gradually formed. Figure 1 shows that the quality of the cross-sectional geometry of large channels increases as we go from rectangle (in this case square) to circle to diamond. However, for channels 1 mm or smaller, the fidelity of the cross-sectional geometry is best for the rectangular shape.

Prevention of Leakage. Leakage is probably the most undesirable phenomenon that a fluidic device can exhibit. Figure 2 demonstrates a number of channels (0.8 mm width × 0.8 mm height) of the exact same geometry, yet sliced with different settings, that are filled with a methanol/water (1:1, v/v) solution containing blue dye. The value of the *infill solidity* parameter determines the ratio between the filament and air in the interior of the part; a value of 0.2 yields a very open infill, whereas 1.0 leads to a complete fill of the internal volume. The *shell number* refers to the number of adjacent filament threads that outline the contours of all structures.

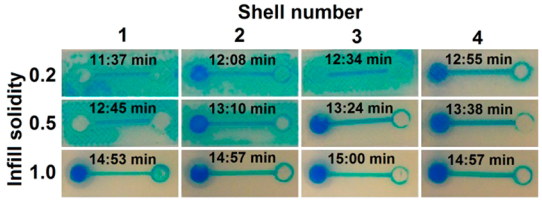

Figure 2. Influence of the infill solidity and shell number on leakage prevention in a 3D-printed channel. The estimated print time (after slicing) is shown for each setting as well. Detailed schematic diagrams are given in Figure S2, Supporting Information.

This figure shows that a more solid infill is preferential for fluidic devices. However, this means a larger consumption of material, as well as increased printing times, as can be seen from the estimated print times, calculated by the software after slicing. Another way to prevent leakage is to increase the shell number. Even with a very open infill (0.2), a shell number of 4 led to a channel exhibiting no leakage into the rest of the part. These settings also result in shorter print jobs compared to high-infill settings.

Transparency. Many microfluidic devices rely on visual (microscopic) inspection for control of their operation. For this reason, materials such as PDMS, glass, and transparent thermoplastics are very popular in the field. Transparency is claimed for a number of FDM materials. As of yet, to the best of our knowledge, 60% transmission (430−620 nm light) through a 500 μm thick polymer layer is the highest level of transparency achieved, but this was done with photocurable resin and DLP.[9] In FDM, not only the transmission of the material itself, but also the microstructure of the produced parts is relevant. Due to the stacking of layers of threads, light is scattered as it passes through a polymer device. When using one of these "transparent" materials, see-through devices can be made, as long as the thickness of the part is kept at a minimum (roughly up to 1 mm). To cope with this, glass slides can be integrated into 3D-printed devices. One possible approach is to fabricate a channel with the 3D printer which is open at the bottom and then attach it with glue or a photocurable resin to the glass slide.[25,27] In this work, we produced a test device with sealed channels that were 3D-printed on top of an embedded glass slide. This glass slide was inserted during the print, after the printer was paused. This is an attractive feature of FDM 3D

DOI: 10.1021/acs.analchem.7b00828
Anal. Chem. 2017, 89, 7053−7061

printing that is not found in SL or DLP approaches. Figure 3 shows the device from the top (Figure 3A, poly(lactic acid),

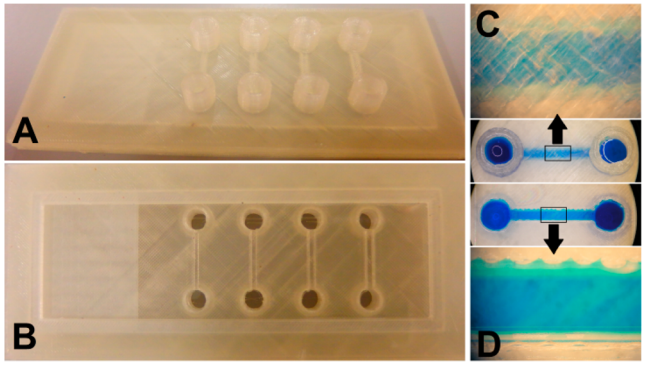

Figure 3. (A, B) PLA−glass device with sealed fluidic channels, suitable for microscopic inspection (see the Supporting Information, Figure S3, for the dimensions). The glass slide is incorporated into a single 3D-printed PLA part. The glass is inserted during the print by pausing the print. (C) Transparent PLA was used, which gives semitransparency through a limited thickness. The thickness of the top PLA layer through which the blue solution is being visualized is 0.8 mm, which is clearly too thick for a clear image of the microchannel (1 mm wide and high). (D) The blue solution in the same printed channel can be clearly imaged under the microscope when viewed through the glass bottom. There appears to be a bit of leakage along the edges of the PLA channel where it contacts the glass slide.

PLA, side) and from the bottom (Figure 3B, glass slide). The channel was then filled with an aqueous solution of blue dye. The thickness of the PLA ceiling over the channel is 0.8 mm. Although the liquid can be observed when the channel is viewed from above (Figure 3C), it is clear that true transparency is not achieved. However, when viewed through the glass slide at the bottom of the channel, we obtained an unobscured view. The obtained channels can confine aqueous solutions and are compatible with microscopy on the glass-slide side. More research is required, however, to quantify and improve the strength of PLA adhesion to the glass, which is weaker than attachment to PLA. When PLA is printed on top of PLA, the layers melt together, which does not happen when printed on glass. Noteworthy is that FDM provides for the incorporation of other materials or components besides glass, such as paper, membranes, and electrodes.

The above-mentioned solution enables transparency in channels with one planar wall (which is the glass slide in this case), but this approach cannot be applied to channels making up 3D networks in a device. However, such channels should only be used when there is a functional demand, since they are more difficult to produce. If such a channel is included in a device for a functional reason, and visual inspection is also needed, a channel with a planar wall (such as a glass slide) can be implemented into the design after this functional element and can be used for visual inspection of the parameter of interest. Alternatively, FDM printing could be used for indirect fabrication of channels that travel through all planes by employing sacrificial templates[31] (described in the section "3D-Printed Masters for PDMS Casting") in a transparent material.

Combining Materials. In addition to the integration of non-3D-printed objects into a part, FDM also allows the fabrication of hybrid devices. Highly complex structures can be obtained by using dual-head printing, in which two materials can be printed more or less simultaneously, thus allowing embedding of one material in the other. A simpler approach is to pause the print at a certain point and exchange the filament. One such example can be found in the combination of PLA with Arnitel in a two-layer part for masking paper during exposure to oxygen plasma.[17] When pressure is applied to the rigid PLA side, the flexible Arnitel side conforms to whatever surface it is in contact with, in this case paper. Using this approach, it was possible to shield paper from exposure to oxygen plasma, as demonstrated in previous work.[17]

Warping. During a print, especially for large, time-consuming parts, the internal temperature of the printed object tends to vary. Materials are printed at high temperature (around 200 °C, the temperature of the extrusion nozzle) onto the print bed (around 60 °C) and cooled with an integrated fan for quick solidification. This usually causes shrinkage and can lead to deformation through warping. Warping can lead to detachment from the print bed and thus compromises part fabrication. Warping can easily become a problem if the temperature of the print bed is too low or if the print bed is not well aligned or is too far from the extruder. Under all these circumstances, initial attachment to the print bed is insufficient. Materials that require higher temperatures for extrusion and bed adhesion are especially prone to warping and detachment (e.g., acrylonitrile butadiene styrene, ABS). There are a number of options to reduce or prevent part detachment due to warping: (i) place the printer in a closed box (preventing convective air movement) that can be heated to maintain a more uniform temperature distribution, (ii) coat the print bed with a material that enhances adhesion (e.g., ABS dissolved in acetone or hairspray), (iii) print the first few layers of the part in a material that has good adhesion to the plate (e.g., PLA soft) and then switch to the actual material for the print, and (iv) have the slicing software include a brim in the G-code for the part, which can be removed after the print is done. Incorporating a brim means that a number of additional shells are printed on the first layer to increase the surface attached to the plate.

Polymers for FDM 3D Printing. The results for the different characterizations performed on 12 FDM materials can be found in Table 1. We refer the reader to Table S2 in the Supporting Information for a list of the printing parameters for these materials. The following sections deal with the different aspects of the materials that need to be taken into account when a material is selected for an application. Note that suppliers of filament (i) generally do not list the exact chemical composition of their filament and (ii) are continuously improving their products, as we are currently going through a phase of rapid development in the 3D printing field.

Polymer Printability. This section describes the problems that might be encountered when the different polymers are printed individually. The success or failure of the print process for a part largely depends on whether the first layer is printed properly. As alluded to in the previous section, warping and/or detachment from the print bed is an important cause for failure. The print bed used in this work can reach a maximum temperature of approximately 80 °C. This means that materials such as ABS, polystyrene (PS), and especially polycarbonate (PC) are difficult to print, as they require higher temperatures for bed adhesion and are thus more prone to warping. For small parts, this can be overcome by printing with a brim, as discussed above. Coating of the print bed with adhesive material also improves attachment, but was not an option for this study, as it would lead to contamination of the test

DOI: 10.1021/acs.analchem.7b00828
Anal. Chem. 2017, 89, 7053−7061

Table 1. Solvent Compatibility, Biocompatibility, and Autofluorescence of 12 FDM Materials[a]

material	composition based on	color	transparency	autofluorescence blue	autofluorescence green	autofluorescence red	water-compatible	methanol-compatible	acetonitrile-compatible	2-propanol-compatible	acetone-compatible	HUVEC-compatible	PCLS-compatible
PLA gold	poly(lactic acid)	gold	none	+	++	+	+	+/−	−−	+	−−	+	+
transparent PLA	poly(lactic acid)	colorless	semi	+	+	+/−	+	+/−	−−	+	−−	+	+
PLA soft	poly(lactic acid)	beige	none	+/−	+	+/−	+	+	+/−	+	+/−	+	+
PLA 45	poly(lactic acid)	white	none	++	+/−	−	+	+/−	−−	+/−	−−	+	+
ABS	acrylonitrile butadiene styrene	orange	none	++	++	++	+	−	−−	+	−−	+	+
PC	polycarbonate	colorless	semi	++	++	++	+	+	−	+	−	+	+
PS	polystyrene	cream	none	++	++	+	+	+	+	+	−−	+	+
PVA	poly(vinyl alcohol)	light yellow	semi	++	++	++	−−	−−	−	−	−−	−	−
PET	poly(ethylene terephthalate)	colorless	semi	++	+	+/−	+	+	−	+	−	+	+
T-Glase	poly(ethylene terephthalate)	colorless	semi	++	+	+/−	+	+	−	+	−	+	+
Arnitel	thermoplastic co-polyester	white	none	++	++	+/−	+	+	+	+	+	+	+
Bendlay	acrylonitrile butadiene styrene	colorless	semi	+	++	+	+	+	−	+	−	+	+

[a]The classification of biocompatibility, solvent compatibility, and autofluorescence is based on the rules for performance described in the Supporting Information (protocol S5, solvent compatibility; protocol S6, biocompatibility; Figure S6, autofluorescence).

DOI: 10.1021/acs.analchem.7b00828
Anal. Chem. 2017, 89, 7053−7061

structures. For the production of PC parts, another temperature-related problem can be encountered, associated with the actual softening of printer components (e.g., poly(ether ether ketone), PEEK, insulation) after prolonged usage at temperatures around 250 °C. This can lead to irreparable damage of the printer component.

Autofluorescence. The autofluorescence of a material refers to its own tendency to emit fluorescence upon illumination with light at certain wavelengths. Autofluorescence can be a limitation when the material is used in tests that rely on fluorescence, especially for quantitative analysis. Table 1 shows to what extent the 12 materials that were tested exhibit autofluorescence at different wavelengths. We defined categories with selected thresholds and classified the materials accordingly. The photographs and numerical data can be found in Figures S5 and S6 of the Supporting Information, respectively. All the materials tested exhibit autofluorescence to some degree, but with some the level is quite acceptable. PLA 45 can be employed when green and red fluorescence are used, whereas PLA soft is applicable to blue and red. In general, the FDM materials tested exhibited less autofluorescence at red wavelengths. The application of fluorescence detection at longer visible (red) wavelengths in a 3D-printed device thus allows for a broader selection of FDM materials. Importantly, some of the tested materials contain (colored) additives, which might influence the level of autofluorescence.

Solvent Compatibility. Table 1 gives an overview of the compatibility of the 12 materials with 5 different solvents. 3D-printed test structures were exposed to the different solvents. The differences after 1 week (168 h) in weight of the structure before and after exposure and the amount of dissolved material in the solvent were determined by weighing the contents of the testing tubes. The materials were then classified into different categories on the basis of these numerical data and photographs after exposure (respectively Figures S7 and S8, Supporting Information). These results demonstrate that all the materials except PVA are compatible with water. 2-Propanol and methanol are both compatible with most materials, but acetonitrile and acetone are more challenging. Arnitel is the only material from this selection which can be employed for all five solvents. Furthermore, it is remarkable that the flexible materials (PLA soft and Bendlay) show better solvent compatibility than the rigid filament on which they are based (PLA and ABS, respectively), which we assume is caused at least in part by additives meant to increase flexibility. Finally, it should be noted that in a few cases the sum of the dissolved weight and remaining weight exceed 100% of the initial weight (see Figure S7). This can potentially be attributed to swelling phenomena and/or encapsulation of solvent in the polymer matrix.

Biocompatibility. Table 1 shows the results of the biocompatibility studies. Out of the 12 FDM materials tested, 11 show biocompatibility with HUVECs and PCLSs (Figures S9−S13, Supporting Information); only PVA shows significant toxicity for both biological models in comparison with the controls ($p = 0.009$ for MTT test in HUVECs, $p = 2 \times 10^{-7}$ for LDH leakage in PCLSs, $p = 0.002$ for ATP measurement in PCLSs). Although PVA is described as a biocompatible material and is used in medical studies,[32] it was toxic in experiments performed with both HUVECs and PCLSs. This may be explained by the high solubility of PVA in the aqueous medium. This leads to an observed increase in the medium viscosity (the medium becomes gel-like), which may result in decreased diffusion of nutrients and oxygen to the cells and hence decreased viability. Furthermore, contaminants or additives might be present in the filament. After dissolution, these might have a toxic effect on the biological material. The fact that the solvent compatibility studies show no dissolution of any of the other materials in water is also in line with the observation that they do not cause a loss in viability in cells or tissue.

A control experiment was carried out to assess the possible influence of the materials on the fluorescence-based LDH assay. It measured the absolute emission intensity in the absence of PCLSs. The only material that caused a significant increase of the intensity measured was PVA ($p = 4 \times 10^{-7}$). However, the average difference from the control was 134 AU, which is less than 1% of the average fluorescence intensity measured in the medium for PCLSs incubated with PVA for 24 h. The effect of PVA itself on the LDH assay can therefore be regarded as negligible.

The assays show similar results in cell and tissue cultures. Futhermore, the results are comparable to those found in earlier studies to assess the biocompatibility of FDM materials[18,25,33]—though this study comprises a broader range of materials. To the best of our knowledge, we observe only one deviation from previous biocompatibility results, namely, for ABS. Hyde and co-workers[18] found that ABS exhibits some toxicity toward human neuroblastoma cells and mouse pituitary cells. It was also shown that ABS influenced the functionality of cortical neurons. We, however, have not observed any negative effects of ABS on the HUVEC or PCLS models. Furthermore, the toxicity of a material might also be attributed to additives in the material, which can vary from producer to producer. While our results can serve as a guideline for selecting a safe material for in vitro cell or tissue studies, researchers in other laboratories and working with other cells or tissue will need to confirm the biocompatibility of their materials for their biological models. Finally, with the possible applications of implantable devices in mind, more extensive, clinical biocompatibility studies are required to test the safety and stability of the materials in vivo.

Applications of FDM 3D Printing. *3D-Printed Masters for PDMS Casting.* The use of 3D printers for the fabrication of masters which can be used for casting PDMS (and other curable materials) has been demonstrated for inkjet printing (down to 100 μm resolution[15]) and DLP (down to 50 μm resolution[13]). Figure 4 shows two FDM-printed masters and the resulting PDMS devices. The smallest channel produced had a width of approximately 300 μm.

Figure 4 also demonstrates that complex architectures are easily achievable (Figure 4E), but that the variation in channel width in such devices is quite substantial. The nominal width of the spirally laid out channel in Figure 4F, made using the master in Figure 4E, is 0.3 mm. However, the width of the dye-filled channel varies roughly between 0.1 and 0.5 mm. Additionally, the base plane of the master suffers from roughness, which is characteristic for FDM 3D printing as discussed earlier. This is replicated in the PDMS cast, which can complicate bonding of parts to a flat surface for sealing. This in turn increases the likelihood of leakage. It is possible to use FDM-printed templates for PDMS replication, but other 3D printing methods are perhaps more suitable for this purpose, depending on the required resolution of the part.

The production of sacrificial templates with 3D printing for replication of microfluidic devices (by dissolution of the polymer after curing) has been reported[31] and is a method

DOI: 10.1021/acs.analchem.7b00828
Anal. Chem. 2017, 89, 7053−7061

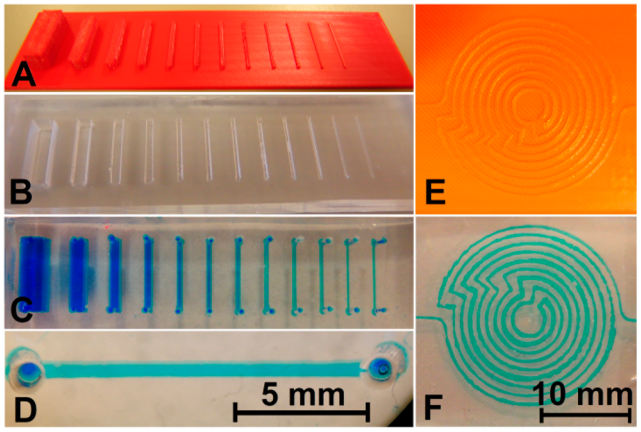

Figure 4. 3D-printed masters for PDMS casting. (A) Master for replication of straight channels (width and height varied between 0.3 and 5.0 mm, aspect ratio of 1). (B) PDMS replicate from the 3D-printed master. (C) Channels were sealed with a PDMS layer and filled with blue solution through holes lining up with the ends of the channel. (D) Expanded view of one of the filled channels. (E) Master for a complex channel. (F) PDMS replicate of the complex channel, filled with blue dye solution.

that can be adapted for FDM. One could print a 3D object in PVA, cast PDMS around it, and later dissolve the PVA in water to remove it. This approach could also circumvent the above-mentioned problem of leakages in the PDMS device due to surface roughness of the master, as the PDMS device could be replicated in a single step.

3D-Printed Channels. Many reports have described the use of 3D-printed channels, some of which employed FDM.[7] Figures 1−3 of this paper show simple examples of embedded channels made with FDM as well. From an applications point of view, FDM 3D printing is suitable for the production of fluidic channels. However, if one is aiming to produce channels with cross sections on the order of 100 μm or less, FDM is currently not the way to go. This is because FDM resolution is limited by the nozzle diameter and therefore by the dimensions of extruded filament threads. 3D-printed channel structures might be employed for cell or tissue culture, though a glass slide needs to be incorporated to allow microscopic examination of the cells. Most of the materials that are used in FDM 3D printing are also biocompatible, which makes this method an excellent choice for development of devices for cell-based applications. Furthermore, FDM-printed channels might be a good option for devices that do not need micrometer dimensions for exact fluid control, such as for simple chemical processes. This is especially true when there are financial or technological restrictions.

Since 3D printing allows the creation of objects of almost any shape, the fluidic entrance can be designed to fit to tubing or other means of coupling to a pumping system. It was demonstrated above that, by only applying hydrostatic pressure, leakage could easily occur in devices with open infill, but also that it could be solved by increasing the shell number or infill solidity. Such aspects need to be taken into consideration during both the design and slice processes.

Patterning in Paper Microfluidics. Hydrophilic channels or lanes can be defined in paper using hydrophobic patterning techniques. Passive fluid transport by capillary action then serves to move liquids through the paper channels to carry out reactions or other sample handling. Hydrophobic patterning may be accomplished in different ways. 3D-printed parts may be used in the production of paper microfluidic structures, as we have reported for the patterning of alkyl ketene dimer-treated paper strips.[17] One other approach which has received some attention in our laboratory involves the use of wax deposition,[34] for which we have developed a tool by FDM 3D printing, as shown in Figure 5. The 3D-printed parts (Figure 5A,B) successfully shielded parts of the paper from the deposition of molten wax when the assembly in Figure 5B was dipped in it. This reproducibly led to clearly defined hydrophilic (untreated paper, white) and hydrophobic (wax-treated, gray) regions (Figure 5C,D). The paper channels defined between the wax barriers were characterized with respect to their width (Figure 5D,E). Correlation was found between the width of the thin PLA strip of the mask and the size of the resulting paper microfluidic channel. 3D printing is very suitable for the realization of rapid prototyping of different paper microfluidic structures. However, for mass production of

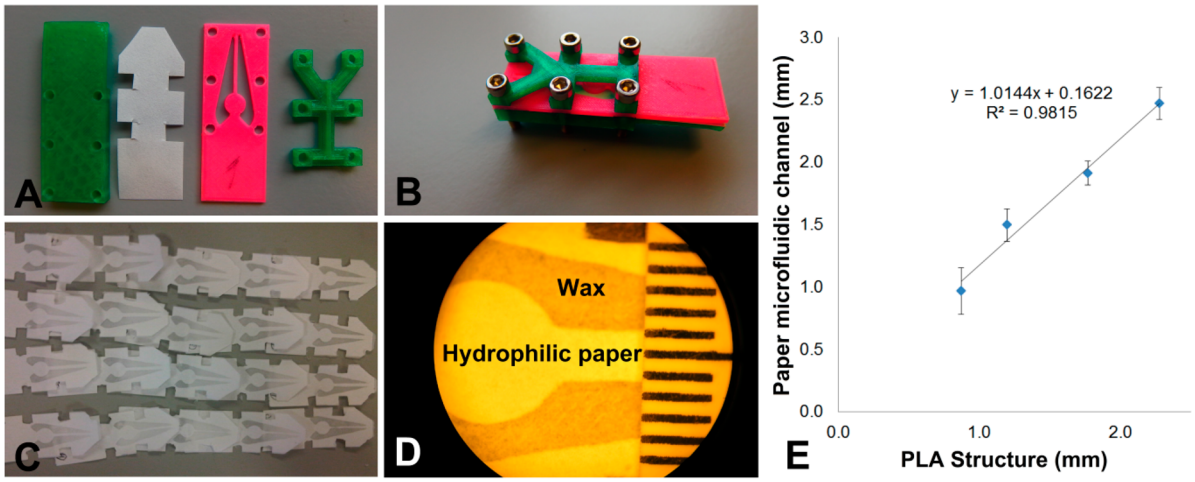

Figure 5. Wax patterning approach that used 3D-printed masks to shield the paper from modification. (A) 3D-printed PLA parts (green and pink) and a strip of paper. (B) Assembly of the parts with the paper strip sandwiched between the green rectangular base and pink mask. (C) Resulting wax patterns on paper. (D) Microscopic image of a wax pattern defining a paper channel (approximately 2 mm wide), with a ruler for size calibration. (E) Correlation between the size of the 3D-printed masks and the actual channel size. Error bars show standard deviations (n = 5 per data point).

DOI: 10.1021/acs.analchem.7b00828
Anal. Chem. 2017, 89, 7053−7061

paper microfluidic devices, other production methods are more time-efficient.

Customizing Laboratory Equipment and 3D-Printed Tools. A last example of the applicability of (FDM) 3D printing for a research laboratory involves the production of labware and lab tools or the customization of an experimental setup, saving money and time and allowing for robust and user-friendly experimental setups. Figure 6 shows a few such applications in our laboratory.

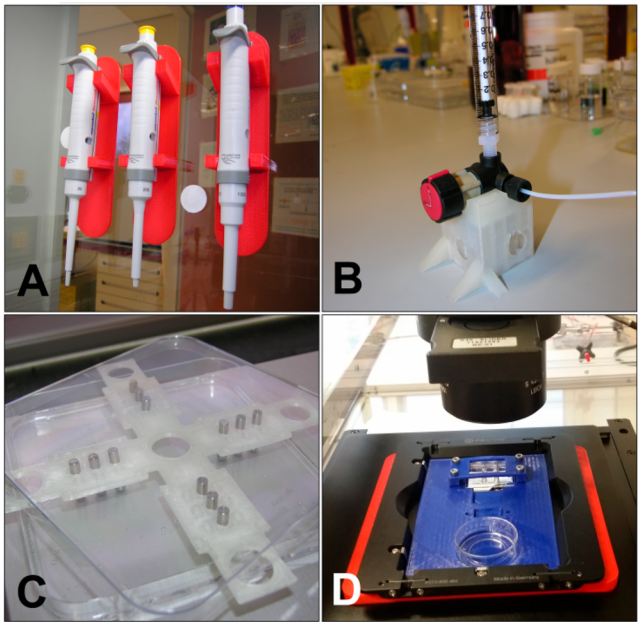

Figure 6. Examples of 3D-printed tools used in a research laboratory. (A) 3D-printed pipet holders (red). (B) 3D-printed stand for a bulky four-way valve (colorless). (C) 3D-printed alignment plate for pins, to create aligned holes when a slab of PDMS is cast (colorless). (D) Customized 3D-printed microscope stage for cell cultivation microchips (blue).

CONCLUSION

In November 2012, we bought a Felix v.1.5 printer for roughly 1.000 €. At that time we had no real expectations of this technology, and it seemed like an interesting and relatively inexpensive experiment. 3D printing was a new concept in the field of lab-on-a-chip and (bio)analytical technology, and few laboratories had experience with this technology. Now, only about 4 years later, we have seen a rapid increase in the number of publications in microfluidics and related fields utilizing this technology. Furthermore, it is now difficult to imagine life in our own laboratory without 3D printing.

3D printing is a technique that belongs to everybody. The advent of affordable printers has meant the rapid establishment of this technology in many aspects of life besides research. The societal impact of the technology has been growing, meaning that further leaps in the development of this tool are likely in the near future. One big advantage of the common appeal of the 3D printer is the fact that there is a large interactive community revolving around this topic. This community has proven to be valuable for the research described in this work, as solutions for some of the described problems (as well as some ideas) were developed after various Internet forums, such as the RepRap forums and various forums linked to commercially available printers (e.g., Felix and Ultimaker), were consulted. Unfortunately, such information is diffuse and almost impossible to trace to the original authors or inventors, so their sources do not appear in the list of references for this work.

In relation to other printing approaches, FDM is probably the most accessible. Both the materials and the printer itself are inexpensive. Other advantages of the FDM method include the ease with which different materials can be switched during a print and the possibility to integrate and embed external components into a single part. Other benefits are the biocompatibility of most FDM materials with tissue and cells and the wide range of materials available for printing. Drawbacks are mainly related to the resolution and surface smoothness (which is slightly better with other 3D printing approaches, such as DLP). However, given the rate of current developments, we expect that (FDM) printers capable of achieving higher resolution will become available in the foreseeable future.

It is our hope that this work, as well as all the work cited, will help to convince researchers in the field of microfluidics and lab-on-a-chip that 3D printing indeed offers grand opportunities to do better, more efficient science. This is certainly a technology that can make our jobs as scientists easier and, moreover, stimulate our creativity.

ASSOCIATED CONTENT

Supporting Information

The Supporting Information is available free of charge on the ACS Publications website at DOI: 10.1021/acs.analchem.7b00828.

Images of the SolidWorks designs for printed parts used in the manuscript, tables with slice and print settings, protocols for all the experiments in this paper, and figures, photographs, and box plots displaying results for the characterization of FDM materials (PDF)

AUTHOR INFORMATION

Corresponding Author

*E-mail: e.m.j.verpoorte@rug.nl.

ORCID

Pieter E. Oomen: 0000-0001-8395-7331

Notes

The authors declare no competing financial interest.

ACKNOWLEDGMENTS

This research received funding from The Netherlands Organization for Scientific Research (NWO) in the framework of the Technology Area Comprehensive Analytical Sciences and Technology (COAST).

REFERENCES

(1) Gross, B. C.; Erkal, J. L.; Lockwood, S. Y.; Chen, C.; Spence, D. M. *Anal. Chem.* **2014**, *86*, 3240−3253.

(2) Ho, C. M. B.; Ng, S. H.; Li, K. H. H.; Yoon, Y.-J. *Lab Chip* **2015**, *15*, 3627−3637.

(3) Au, A. K.; Huynh, W.; Horowitz, L. F.; Folch, A. *Angew. Chem., Int. Ed.* **2016**, *55*, 3862−3881.

(4) Zhang, C.; Bills, B. J.; Manicke, N. E. *Bioanalysis* **2017**, *9*, 329−331.

(5) Yazdi, A. A.; Popma, A.; Wong, W.; Nguyen, T.; Pan, Y.; Xu, J. *Microfluid. Nanofluid.* **2016**, *20*, 50.

DOI: 10.1021/acs.analchem.7b00828
Anal. Chem. 2017, 89, 7053−7061

(6) Waheed, S.; Cabot, J. M.; Macdonald, N. P.; Lewis, T.; Guijt, R. M.; Paull, B.; Breadmore, M. C. *Lab Chip* **2016**, *16*, 1993−2013.
(7) Kitson, P. J.; Rosnes, M. H.; Sans, V.; Dragone, V.; Cronin, L. *Lab Chip* **2012**, *12*, 3267−3271.
(8) Anderson, K. B.; Lockwood, S. Y.; Martin, R. S.; Spence, D. M. *Anal. Chem.* **2013**, *85*, 5622−5626.
(9) Shallan, A. I.; Smejkal, P.; Corban, M.; Guijt, R. M.; Breadmore, M. C. *Anal. Chem.* **2014**, *86*, 3124−3130.
(10) Femmer, T.; Jans, A.; Eswein, R.; Anwar, N.; Moeller, M.; Wessling, M.; Kuehne, A. J. C. *ACS Appl. Mater. Interfaces* **2015**, *7*, 12635−12638.
(11) Krejcova, L.; Nejdl, L.; Rodrigo, M. A. M.; Zurek, M.; Matousek, M.; Hynek, D.; Zitka, O.; Kopel, P.; Adam, V.; Kizek, R. *Biosens. Bioelectron.* **2014**, *54*, 421−427.
(12) Salentijn, G. IJ.; Permentier, H. P.; Verpoorte, E. *Anal. Chem.* **2014**, *86*, 11657−11665.
(13) Comina, G.; Suska, A.; Filippini, D. *Lab Chip* **2014**, *14*, 424−430.
(14) Chan, H. N.; Chen, Y.; Shu, Y.; Chen, Y.; Tian, Q.; Wu, H. *Microfluid. Nanofluid.* **2015**, *19*, 9−18.
(15) Hwang, Y.; Paydar, O. H.; Candler, R. N. *Sens. Actuators, A* **2015**, *226*, 137−142.
(16) Bonyár, A.; Sántha, H.; Varga, M.; Ring, B.; Vitéz, A.; Harsányi, G. *Int. J. Mater. Form.* **2014**, *7*, 189−196.
(17) Salentijn, G. IJ.; Hamidon, N. N.; Verpoorte, E. *Lab Chip* **2016**, *16*, 1013−1021.
(18) Hyde, J.; MacNicol, M.; Odle, A.; Garcia-Rill, E. *J. Neurosci. Methods* **2014**, *238*, 82−87.
(19) Paydar, O. H.; Paredes, C. N.; Hwang, Y.; Paz, J.; Shah, N. B.; Candler, R. N. *Sens. Actuators, A* **2014**, *205*, 199−203.
(20) Kitson, P. J.; Marshall, R. J.; Long, D.; Forgan, R. S.; Cronin, L. *Angew. Chem., Int. Ed.* **2014**, *53*, 12723−12728.
(21) Lücking, T. H.; Sambale, F.; Schnaars, B.; Bulnes-Abundis, D.; Beutel, S.; Scheper, T. *Eng. Life Sci.* **2015**, *15*, 57−64.
(22) Lücking, T. H.; Sambale, F.; Beutel, S.; Scheper, T. *Eng. Life Sci.* **2015**, *15*, 51−56.
(23) Ude, C.; Hentrop, T.; Lindner, P.; Lücking, T. H.; Scheper, T.; Beutel, S. *Sens. Actuators, B* **2015**, *221*, 1035−1043.
(24) Tyson, A. L.; Hilton, S. T.; Andreae, L. C. *Int. J. Pharm.* **2015**, *494*, 651−656.
(25) Wardyn, J. D.; Sanderson, C.; Swan, L. E.; Stagi, M. *J. Neurosci. Methods* **2015**, *251*, 17−23.
(26) Zwicker, A. P.; Bloom, J.; Albertson, R.; Gershman, S. *Am. J. Phys.* **2015**, *83*, 281−285.
(27) Takenaga, S.; Schneider, B.; Erbay, E.; Biselli, M.; Schnitzler, T.; Schöning, M. J.; Wagner, T. *Phys. Status Solidi A* **2015**, *212*, 1347−1352.
(28) Van Midwoud, P. M.; Groothuis, G. M. M.; Merema, M. T.; Verpoorte, E. *Biotechnol. Bioeng.* **2010**, *105*, 184−194.
(29) Van Kooten, T. G.; Klein, C. L.; Köhler, H.; Kirkpatrick, C. J.; Williams, D. F.; Eloy, R. *J. Mater. Sci.: Mater. Med.* **1997**, *8*, 835−841.
(30) Comina, G.; Suska, A.; Filippini, D. *Lab Chip* **2014**, *14*, 2978−2982.
(31) Gelber, M. K.; Bhargava, R. *Lab Chip* **2015**, *15*, 1736−1741.
(32) Baker, M. I.; Walsh, S. P.; Schwartz, Z.; Boyan, B. D. *J. Biomed. Mater. Res., Part B* **2012**, *100B*, 1451−1457.
(33) Macdonald, N. P.; Zhu, F.; Hall, C. J.; Reboud, J.; Crosier, P. S.; Patton, E. E.; Wlodkowic, D.; Cooper, J. M. *Lab Chip* **2016**, *16*, 291−297.
(34) Songjaroen, T.; Dungchai, W.; Chailapakul, O.; Laiwattanapaisal, W. *Talanta* **2011**, *85*, 2587−2593.

DOI: 10.1021/acs.analchem.7b00828
Anal. Chem. 2017, 89, 7053−7061